Acta Cryst E CRYSTALLOGRAPHIC COMMUNICATIONS

ISSN 2056-9890

Synthesis, crystal structure, Hirshfeld surface analysis, and energy framework of bis{3-(4-bromophenyl)-5-[6-(1*H*-pyrazol-1-yl)pyridin-2-yl]-4*H*-1,2,4-triazol-4-ido}nickel(II) methanol disolvate and comparison with its chloro-substituted analogue

Kateryna Znovjyak,[a] Sergiu Shova,[b] Sergiy O. Nikitin,[c] Yurii S. Moroz,[a] Oksana Tananaiko,[a] Sergey O. Malinkin[a] and Maksym Seredyuk[a]*

[a]Department of Chemistry, Taras Shevchenko National University of Kyiv, Volodymyrska Street 64, Kyiv, 01601, Ukraine, [b]Department of Inorganic Polymers, "Petru Poni" Institute of Macromolecular Chemistry, Romanian Academy of Science, Aleea Grigore Ghica Voda 41-A, Iasi, 700487, Romania, and [c]ChemBioCenter, Kyiv National Taras Shevchenko University, Kyiv 02094, 61 Winston Churchill Street, Ukraine. *Correspondence e-mail: mlseredyuk@gmail.com

Received 28 July 2025
Accepted 20 August 2025

Edited by F. F. Ferreira, Universidade Federal do ABC, Brazil

Keywords: crystal structure; nickel(II) complexes; neutral complexes.

CCDC reference: 2481668

Supporting information: this article has supporting information at journals.iucr.org/e

The unit cell of the title compound, $[Ni(C_{16}H_{10}BrN_6)_2]\cdot 2CH_3OH$, contains a neutral complex and two methanol molecules. The Ni^{II} ion adopts a pseudo-octahedral geometry, coordinated by two tridentate ligands *via* pyrazole, pyridine, and triazole N atoms. The average Ni—N bond length is 2.097 (4) Å. In the crystal, molecules form supramolecular chains through weak C–H···π interactions and further assemble into diperiodic layers *via* C—H···N/C interactions. Hirshfeld surface analysis shows H···H (32.1%), H···C/C···H (27.3%), H···N/N···H (14.9%), and H···Br/Br···H (14.6%) contacts. Interaction energies were evaluated using HF/3–21 G energy frameworks analysis. Structural parameters were compared to those of the chloro-containing analogue, and the effect of substituent variation was discussed.

1. Chemical context

A significant category of coordination compounds comprises 3*d*-metal complexes coordinated with tridentate bisazolepyridine ligands (Halcrow *et al.*, 2019; Suryadevara *et al.*, 2022), which have been employed in diverse applications including catalysis (Xing *et al.*, 2014; Wei *et al.*, 2015) and molecular magnetism (Suryadevara *et al.*, 2022). Recently, we reported an Ni^{II} complex incorporating an asymmetric deprotonated chloro-substituted ligand, 3-(4-chlorophenyl)-5-[6-pyrazolyl(2-pyridyl)]-1*H*-1,2,4-triazole (KULRIW; Znovjyak *et al.*, 2024).

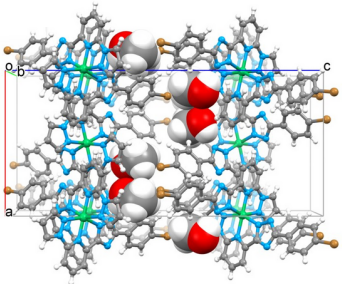

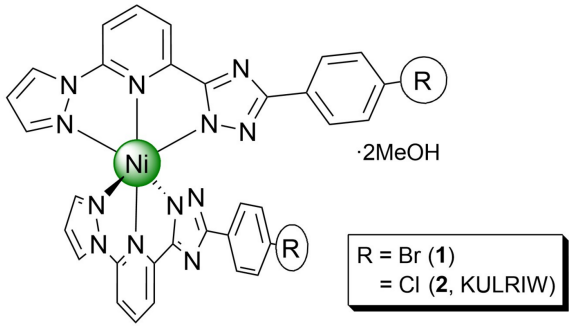

In this study, we describe the synthesis and crystal structure determination of a new complex (**1**) featuring a bromo-

OPEN ACCESS
Published under a CC BY 4.0 licence

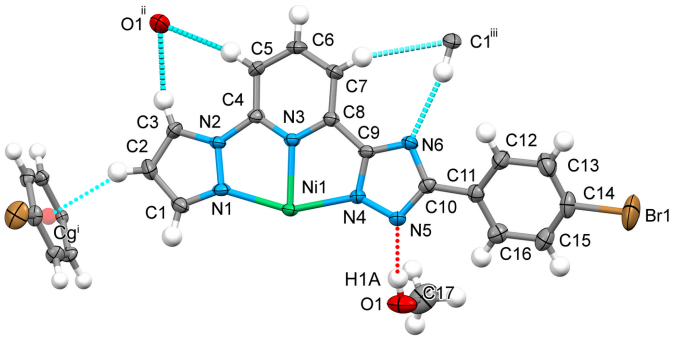

Figure 1
The molecular structure in the asymmetric unit of the title compound and contact atoms with displacement ellipsoids drawn at the 50% probability level. The strong O—H···N (red) and weak C—H···N/C/O/*Cg* (cyan) hydrogen bonds are shown with the nearest neighbors. Symmetry codes: (i) $1-x, 1+y, \frac{3}{2}-z$; (ii) $\frac{1}{2}+x, \frac{1}{2}+y, \frac{3}{2}-z$; (iii) $\frac{1}{2}+x, -\frac{1}{2}+y, \frac{3}{2}-z$.

substituted ligand, 3-(4-bromophenyl)-5-(6-pyrazolyl(2-pyridyl))-1*H*-1,2,4-triazole. Comprehensive structural analyses were performed and the resulting calculated parameters were compared with those of the chloro-derivative (**2**).

2. Structural commentary

The two tridentate ligands span meridional and perpendicular coordination sites on the octahedron, forming a molecule with a compact coordination part and pending diverging 4-bromophenyl groups. The pendant group is tilted by 26.6 (2)° relative to the nearly planar pyrazole-pyridine-triazole (pz-py-trz) fragment (r.m.s. deviation = 0.074 Å). A methanol molecule forms an O—H···N5 hydrogen bond with the triazole ring of the ligand (Table 1, Fig. 1). The central Ni ion adopts a distorted octahedral N_6 coordination sphere, formed by nitrogen atoms from two tridentate ligands, with an average Ni—N bond length of 2.097 (4) Å. The [NiN_6] coordination polyhedron has a volume of 11.616 Å^3. The trigonal distortion parameters are $\Sigma = 119.3°$ ($\Sigma = \Sigma_1^{12}(|90-\varphi_i|)$, where φ_i is the N—Ni—N′ angle; Drew *et al.*, 1995) and $\Theta = 386.9°$ ($\Theta = \Sigma_1^{24}(|60-\theta_i|)$, where θ_i is the angle from superposed opposite octahedral faces; Chang *et al.*, 1990), indicating deviation from ideal octahedral geometry ($\Sigma = \Theta = 0$). The continuous shape measure [CShM(O_h)] relative to ideal octahedral symmetry is 3.702 (Kershaw Cook *et al.*, 2015). Compared to **2**, compound **1** shows marginally higher distortion indices, reflecting the effect of varying pendant substituents (Table 2).

Table 1
Hydrogen-bond geometry (Å, °).

Cg is the centroid of the C11–C16 ring.

D—H···*A*	*D*—H	H···*A*	*D*···*A*	*D*—H···*A*
C3—H3···O1^{i}	0.95	2.35	3.269 (8)	162
C5—H5···O1^{i}	0.95	2.48	3.413 (7)	167
C1—H1···N6^{ii}	0.95	2.30	3.238 (6)	171
C7—H7···C1^{iii}	0.95	2.71	3.615 (7)	161
O1—H1*A*···N5	0.73 (6)	2.08 (6)	2.798 (6)	168 (6)
C2—H2···*Cg*^{iv}	0.95	2.69	3.542 (6)	140

Symmetry codes: (i) $x+\frac{1}{2}, y+\frac{1}{2}, -z+\frac{3}{2}$; (ii) $x-\frac{1}{2}, y+\frac{1}{2}, -z+\frac{3}{2}$; (iii) $x+\frac{1}{2}, y-\frac{1}{2}, -z+\frac{3}{2}$; (iv) $-x+1, y+1, -z+\frac{3}{2}$.

3. Supramolecular features

The title compound exhibits a packing similar to **2**, with adjacent molecules interlocked and interacting *via* weak off-

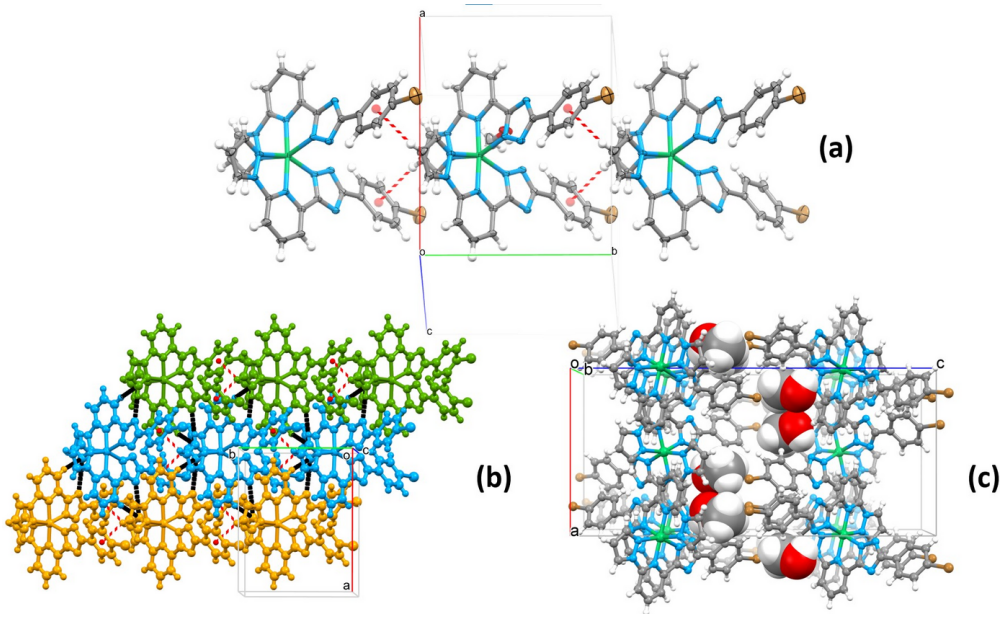

Figure 2
(*a*) A fragment of a monoperiodic supramolecular column formed by stacking of molecules along the *b* axis, with C—H···*Cg* contacts indicated by red dashed lines; (*b*) supramolecular diperiodic layers formed by stacking supramolecular columns in the *ab* plane. The C—H···N/C contacts between chains are indicated by black dashed cylinders. For a better representation, each column has a different color; (*c*) stacking of the diperiodic layers along the *c* axis with the methanol molecules in the voids.

Table 2
Computed distortion indices for the title compound and for similar complexes reported in the literature.

CSD refcode	<*M*—N> (Å)	Σ (°)	Θ (°)	CShM(O_h)
1	2.097	119.3	386.9	3.70
2_(KULRIW)	2.095	119.4	387.3	3.71
YOCFAZ	2.088[a]	120.8[a]	397.6[a]	3.65[a]
ZOCKOT	2.086	121.0	375.9	3.78
ZOTVIP	2.110	124.9	382.4	3.55

Note: (*a*) averaged value.

center non-perpendicular (73.0° angle) C—H(pz)···π(ph) contact between the pyrazole and phenyl groups [H2/C2···*Cg*(ph) = 2.686 (1)/3.542 (6) Å]. The formed one-dimensional chains extend along the *b*-axis direction with a periodicity of 10.1729 (4) Å (Fig. 2*a*), and are linked into corrugated layers in the *ab* plane by weak C—H(pz, py)···N/C(pz, trz) interactions [3.238 (6)–3.746 (7) Å; Fig. 2*b*]. The layers stack without interactions below the van der Waals radii, while methanol molecules occupy the interlayer voids and connect them through weak O···H—C(pz,py) interactions (Fig. 2*c*). Table 1 provides a summary of all intermolecular interactions. Compared to **2**, the overall packing remains similar, with minor differences in the values of intermolecular contacts, which can be compared using Hirshfeld surface analysis.

4. Hirshfeld surface and two-dimensional fingerprint plots

A Hirshfeld surface analysis was conducted and two-dimensional fingerprint plots were generated using *CrystalExplorer 21.5* (Spackman *et al.*, 2021), with a standard resolution for the three-dimensional d_{norm} surfaces plotted over a fixed color scale ranging from −0.6304 (red) to 1.6516 (blue) a.u. Red spots indicate short contacts and negative d_{norm} values on the surface, which correspond to the interactions described above. A projection of d_{norm} mapped over the Hirshfeld surfaces is presented in Fig. 3*a*. The two-dimensional fingerprint plots, along with their relative contributions to the Hirshfeld surface mapped over d_{norm}, are shown in Fig. 4*a*. H···H interactions

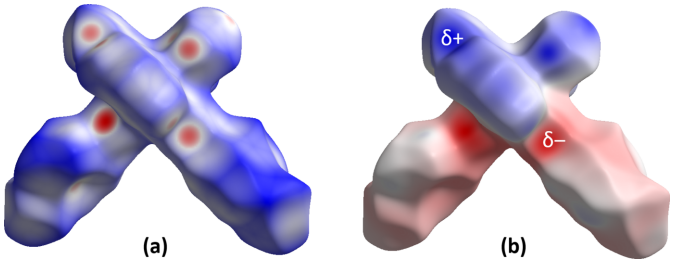

Figure 3
(*a*) A projection of d_{norm} mapped on Hirshfeld surfaces, showing the intermolecular interactions within the molecule. Red/blue and white areas represent regions where contacts are shorter/larger than the sum and close to the sum of the van der Waals radii, respectively. (*b*) Electrostatic potential for the title compound mapped on the Hirshfeld surface. Red/blue and white areas represent regions where the charge is negative/positive or close to zero.

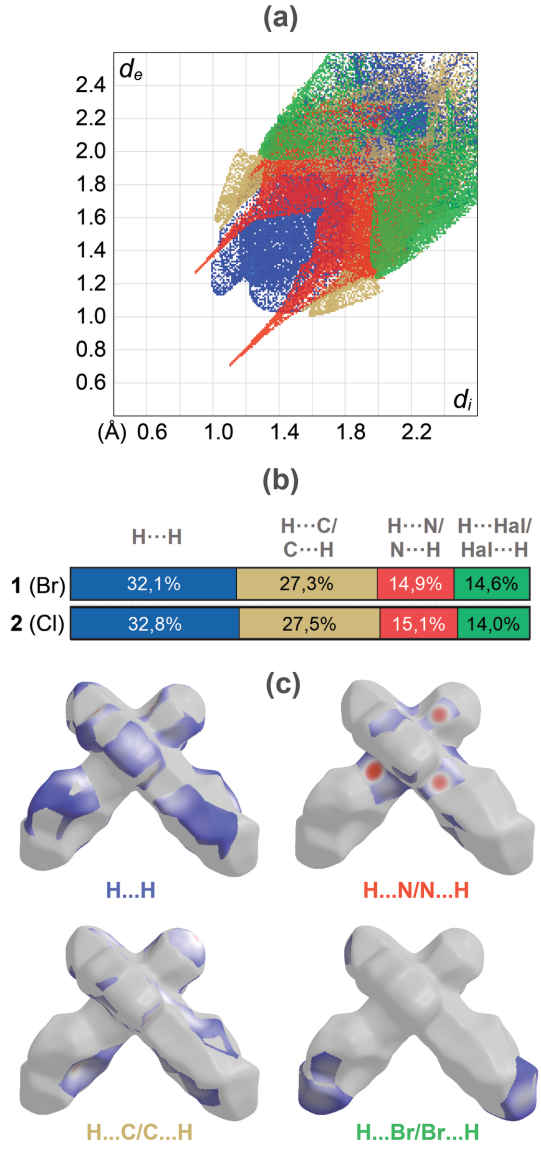

Figure 4
(*a*) Decomposition of the two-dimensional fingerprint plot of **1** into specific interactions and (*b*) comparison with those in **2**; (*c*) a projection of d_{norm} mapped on the Hirshfeld surfaces, showing the intermolecular interactions within the molecule. Red/blue and white areas represent regions where contacts are shorter/larger than the sum and close to the sum of the van der Waals radii, respectively.

account for the largest contribution to the overall crystal packing at 32.1%, and are situated in the middle region of the fingerprint plot. H···C/C···H contacts contribute 27.3%, while H···N/N···H contacts, seen as a pair of sharp spikes, represent a 14.9% contribution to the surface. Interactions of H···Br/Br···H make up 14.6%, forming pairs of characteristic wings. This is greater than the H···Cl/Cl···H interaction in **2**, while other contributions are smaller due to the larger van der Waals radius of Br compared to Cl (1.85 *vs* 1.75 Å; Bondi, 1964) and the corresponding relative contribution to the surface area of the molecule. In Fig. 4*b*, the percentage contribution of contacts to the Hirshfeld surface for the two compounds is compared. In Fig. 4*c*, the different interactions are plotted onto the Hirshfeld surface. The electrostatic

potential energy calculated using the HF/3-21G basis is shown in Fig. 3*b*. The negative charge is localized on the trz-ph moiety and the Br atom of the complex molecule, whereas the pz-py moieties exhibit relatively positive charges, supporting the stacking of molecules into columns and the arrangement of these columns into diperiodic two-dimensional layers.

5. Energy framework analysis

The energy framework (Spackman *et al.*, 2021), calculated at the HF/3-21G level, includes electrostatic (E_{ele}), polarization (E_{pol}), dispersion (E_{dis}), repulsion (E_{rep}) components and total energy (E_{tot}). Cylindrical radii are scaled to the relative strength. Dispersion forces dominate in the crystal of neutral molecules, and the framework topology reflects the described intra- and interlayer interactions. Calculated E_{tot} values are -49.7 kJ mol^{-1} (intrachain), down to -96.5 kJ mol^{-1} (interchain), and -27.0 kJ mol^{-1} (interlayer). Color-coded interaction mappings and detailed energy contributions within 3.8 Å of a central molecule are summarized in Fig. 5*a*–*c*. Fig. 5*d* presents a bar plot comparing the E_{tot} values of **1** and **2**. Despite identical molecular structures and packing arrangements, variations in the size and electronegativity of halogen substituents account for the differing strengths of intermolecular interactions in the two compounds. Consequently, interactions within a supramolecular layer are stronger in **1**, whereas the interlayer interactions are comparatively weaker.

6. Database survey

A search of the Cambridge Structural Database (CSD, Version 5.42; Groom *et al.*, 2016) identifies neutral Ni complexes with tridentate bisazolpyridine ligands containing deprotonable azole groups, such as YOCFAZ (Yuan *et al.*, 2014), ZOCKOT (Xing *et al.*, 2014), and ZOTVIP (Wei *et al.*, 2015). Table 2 summarizes the structural parameters of these complexes along with complex **2** (KULRIW).

7. Synthesis and crystallization

The ligand was synthesized by a modified procedure reported earlier (Seredyuk *et al.*, 2022), and the synthesis of the title complex followed the method of **2** (Znovjyak *et al.*, 2024). All chemicals were purchased from commercial suppliers and used without further purification (Merck, Enamine Ltd.).

3-(4-Bromophenyl)-5-(6-pyrazolyl(2-pyridyl))-1*H*-1,2,4-triazole (***L***). A Schlenk flask with an inert atmosphere was charged with 6-(1*H*-pyrazol-1-yl)pyridin-2-ylboronic acid, (1.00 g, 5.3 mmol), 5-iodo-3-(4-bromophenyl)-1-(tetrahydro-2*H*-pyran-2-yl)-1*H*-1,2,4-triazole (2.09 g, 4.8 mmol),

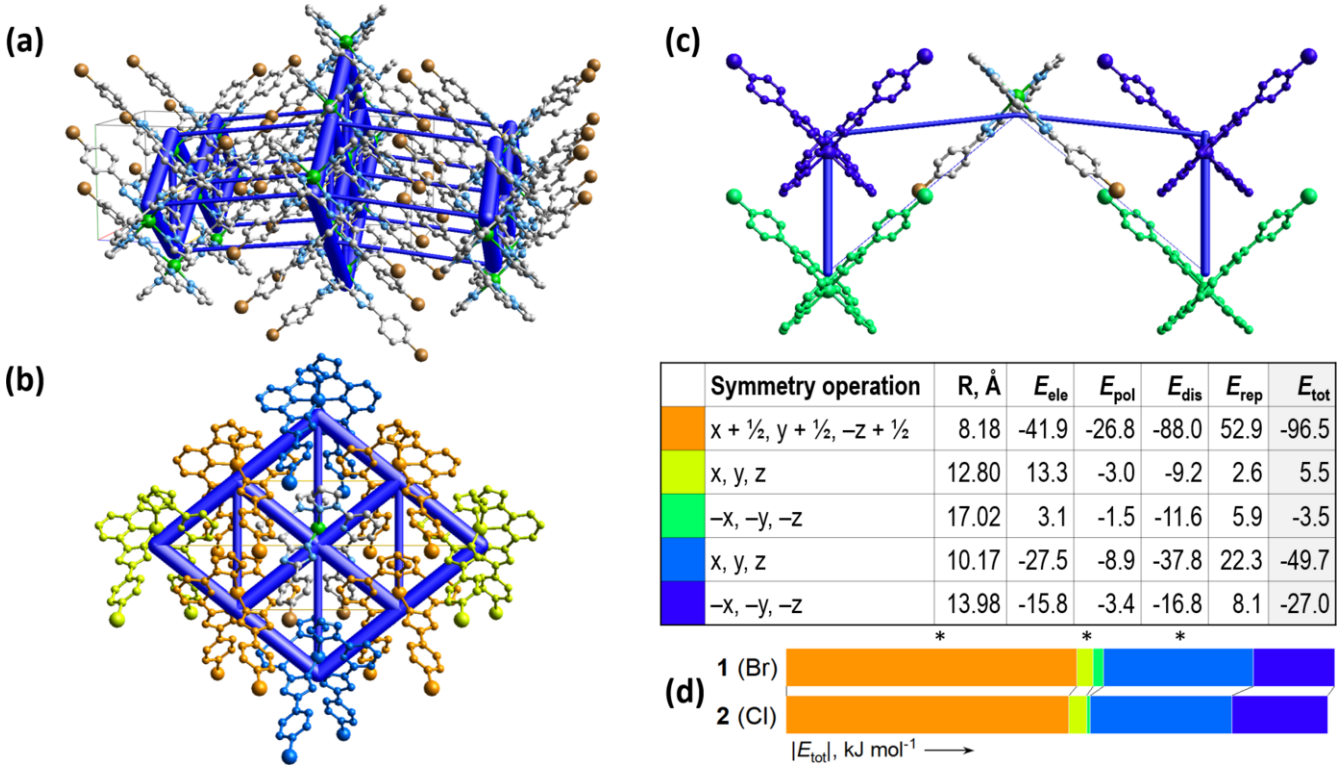

	Symmetry operation	R, Å	E_{ele}	E_{pol}	E_{dis}	E_{rep}	E_{tot}
	x + ½, y + ½, –z + ½	8.18	-41.9	-26.8	-88.0	52.9	-96.5
	x, y, z	12.80	13.3	-3.0	-9.2	2.6	5.5
	–x, –y, –z	17.02	3.1	-1.5	-11.6	5.9	-3.5
	x, y, z	10.17	-27.5	-8.9	-37.8	22.3	-49.7
	–x, –y, –z	13.98	-15.8	-3.4	-16.8	8.1	-27.0

Figure 5
(*a*) The calculated energy frameworks, showing the total energy diagrams (E_{tot}), (*b*) decomposition of the energy framework into the part corresponding to the interactions within a supramolecular layer and (*c*) interlayer interactions. In the table, the corresponding color-coded energy values E_{tot} are provided, including their E_{ele}, E_{pol}, E_{dis}, and E_{rep} components. Tube size is set at 100 scale, the blue color corresponds to the attractive interactions, yellow to the repulsive interactions; (*d*) Comparative plots of the absolute E_{tot} values for **1** and **2**. The color-coding of the bars corresponds to the symmetry operations in the table above. The asterisks distinguish the energy bars corresponding to the intralayer interactions.

Table 3
Experimental details.

Crystal data	
Chemical formula	$[Ni(C_{16}H_{10}BrN_6)_2]\cdot 2CH_4O$
M_r	855.21
Crystal system, space group	Orthorhombic, *Pbcn*
Temperature (K)	200
a, *b*, *c* (Å)	12.8038 (8), 10.1729 (4), 27.9377 (14)
V (Å^3)	3638.9 (3)
Z	4
Radiation type	Mo *Kα*
μ (mm^{-1})	2.78
Crystal size (mm)	0.3 × 0.2 × 0.03
Data collection	
Diffractometer	Xcalibur, Eos
Absorption correction	Multi-scan (*CrysAlis PRO*; Rigaku OD, 2024)
T_{min}, T_{max}	0.534, 1.000
No. of measured, independent and observed [$I > 2\sigma(I)$] reflections	11620, 3218, 2074
R_{int}	0.064
(sin $\theta/\lambda)_{max}$ (Å^{-1})	0.595
Refinement	
$R[F^2 > 2\sigma(F^2)]$, $wR(F^2)$, *S*	0.061, 0.134, 1.04
No. of reflections	3218
No. of parameters	236
H-atom treatment	H atoms treated by a mixture of independent and constrained refinement
$\Delta\rho_{max}$, $\Delta\rho_{min}$ (e Å^{-3})	0.74, −0.81

Computer programs: *CrysAlis PRO* 1.171.43.124 (Rigaku OD, 2024), *SHELXT* (Sheldrick, 2015*a*), *SHELXL2018/3* (Sheldrick, 2015*b*) and *OLEX2* (Dolomanov *et al.*, 2009).

$[Pd(PPh_3)_4]$ (0.61 g, 0.53 mmol) and Na_2CO_3 (1.65 g, 15.6 mmol). Degassed 1,4-dioxane (20 mL) and degassed water (10 mL) were added, and the reaction mixture was heated to 373 K under vigorous stirring for 16 h. After filtering through a Celite pad, to the obtained solution HCl_{aq} (37%, 5 ml) was added dropwise and the obtained solution was stirred for 10 min. Thereafter the pH of the solution was brought to neutral with an aqueous solution of NaOH (10%). The resulting suspension was evaporated to dryness and resuspended in water, and the precipitate was collected by filtration, washed with water and recrystallized from chloroform-acetone (1:1). After drying *in vacuo*, the final compound was isolated as an analytically pure white crystalline powder. Yield: 1.02 g, 57%. Elemental analysis calculated for $C_{16}H_{11}BrN_6$: C, 52.34; H, 3.02; N, 22.89. Found: C, 52.12; H, 3.11; N, 22.62. ^{1}H NMR (300 MHz, 298 K, DMSO-d_6): δ (ppm) 14.90 (1H, *s*, trzH), 9.16 (1H, *s*, pzH), 8.12–7.96 (5H, *m*, phH/pyH), 7.83 (1H, *s*, pzH), 7.64 (2H, *d*, J = 8.4 Hz, phH), 6.62 (1H, *s*, pzH). ^{13}C NMR (75 MHz, DMSO-d_6): δ (ppm) 161.5, 154.5, 150.9, 144.7, 143.0, 141.4, 132.1, 130.7, 128.7, 128.3, 122.9, 118.8, 113.1, 108.7.

Complex **1** was produced by a layering technique in a standard test tube. The layering sequence was as follows: the bottom layer contained a solution of $[Ni(L_2)](ClO_4)_2$ prepared by dissolving *L* (101 mg, 0.274 mmol) and $Ni(ClO_4)_2\cdot 6H_2O$ (50 mg, 0.137 mmol) in boiling acetone, to which chloroform (5 ml) was then added. The middle layer was a methanol–chloroform mixture (1:10, 10 ml), which was covered by a layer of methanol (10 ml), to which 5 drops of NEt_3 were added. The tube was sealed, and light violet plate-like single crystals appeared after 2 weeks (yield *ca.* 65%). Elemental analysis calculated for $C_{34}H_{28}Br_2N_{12}NiO_2$: C, 47.75; H, 3.30; N, 19.65. Found: C, 47.52; H, 3.41; N, 19.73.

8. Refinement

Crystal data, data collection and structure refinement details are summarized in Table 3. H atoms were refined as riding [C—H = 0.95–0.98 Å with U_{iso}(H) = 1.2–1.5U_{eq}(C)]. The hydrogen atom H1*A* was refined freely.

Acknowledgements

The authors are grateful to the FAIRE programme provided by the Cambridge Crystallographic Data Centre (CCDC) for the opportunity to use the Cambridge Structural Database (CSD) and associated software. Author contributions are as follows: Conceptualization, KZ and MS; methodology, KZ; formal analysis, SON; synthesis, SOM; single-crystal measurements, SS; writing (original draft), MS; writing (review and editing of the manuscript), OT, MS; visualization and calculations, KZ, YSM; funding acquisition, MS.

Funding information

Funding for this research was provided by: grants from the Ministry of Education and Science of Ukraine (grant No. 24BF037-03).

References

Bondi, A. (1964). *J. Phys. Chem.* **68**, 441–451.
Chang, H. R., McCusker, J. K., Toftlund, H., Wilson, S. R., Trautwein, A. X., Winkler, H. & Hendrickson, D. N. (1990). *J. Am. Chem. Soc.* **112**, 6814–6827.
Dolomanov, O. V., Bourhis, L. J., Gildea, R. J., Howard, J. A. K. & Puschmann, H. (2009). *J. Appl. Cryst.* **42**, 339–341.
Drew, M. G. B., Harding, C. J., McKee, V., Morgan, G. G. & Nelson, J. (1995). *J. Chem. Soc. Chem. Commun.* pp. 1035–1038.
Groom, C. R., Bruno, I. J., Lightfoot, M. P. & Ward, S. C. (2016). *Acta Cryst.* B**72**, 171–179.
Halcrow, M. A., Capel Berdiell, I., Pask, C. M. & Kulmaczewski, R. (2019). *Inorg. Chem.* **58**, 9811–9821.
Kershaw Cook, L. J., Mohammed, R., Sherborne, G., Roberts, T. D., Alvarez, S. & Halcrow, M. A. (2015). *Coord. Chem. Rev.* **289**, 2–12.
Rigaku OD (2024). *CrysAlis PRO*. Rigaku Oxford Diffraction, Yarnton, England.
Seredyuk, M., Znovjyak, K., Valverde-Munoz, F. J., da Silva, I., Munoz, M. C., Moroz, Y. S. & Real, J. A. (2022). *J. Am. Chem. Soc.* **144**, 14297–14309.
Sheldrick, G. M. (2015*a*). *Acta Cryst.* A**71**, 3–8.
Sheldrick, G. M. (2015*b*). *Acta Cryst.* C**71**, 3–8.
Spackman, P. R., Turner, M. J., McKinnon, J. J., Wolff, S. K., Grimwood, D. J., Jayatilaka, D. & Spackman, M. A. (2021). *J. Appl. Cryst.* **54**, 1006–1011.
Suryadevara, N., Mizuno, A., Spieker, L., Salamon, S., Sleziona, S., Maas, A., Pollmann, E., Heinrich, B., Schleberger, M., Wende, H., Kuppusamy, S. K. & Ruben, M. (2022). *Chem. Eur. J.* **28**, e202103853.

Wei, S. Y., Wang, J. L., Zhang, C. S., Xu, X.-T., Zhang, X. X., Wang, J. X. & Xing, Y.-H. (2015). *ChemPlusChem* **80**, 549–558.

Xing, N., Xu, L. T., Liu, X., Wu, Q., Ma, X. T. & Xing, Y. H. (2014). *ChemPlusChem* **79**, 1198–1207.

Yuan, L.-Z., Ge, Q., Zhao, X.-F., Ouyang, Y., Li, S.-H., Xie, C.-Z. & Xu, J.-Y. (2014). *Synth. React. Inorg. Met.-Org. Nano-Met. Chem.* **44**, 1175–1182.

Znovjyak, K., Shova, S., Panov, D. M., Kariaka, N. S., Fritsky, I. O., Malinkin, S. O. & Seredyuk, M. (2024). *Acta Cryst.* E**80**, 1235–1239.

supporting information

Acta Cryst. (2025). E**81**, 906-911 [https://doi.org/10.1107/S2056989025007467]

Synthesis, crystal structure, Hirshfeld surface analysis, and energy framework of bis{3-(4-bromophenyl)-5-[6-(1*H*-pyrazol-1-yl)pyridin-2-yl]-4*H*-1,2,4-triazol-4-ido}nickel(II) methanol disolvate and comparison with its chloro-substituted analogue

Kateryna Znovjyak, Sergiu Shova, Sergiy O. Nikitin, Yurii S. Moroz, Oksana Tananaiko, Sergey O. Malinkin and Maksym Seredyuk

Computing details

Bis{3-(4-bromophenyl)-5-[6-(1*H*-pyrazol-1-yl)pyridin-2-yl]-4*H*-1,2,4-triazol-4-ido}nickel(II) methanol disolvate

Crystal data

$[Ni(C_{16}H_{10}BrN_6)_2]\cdot 2CH_4O$
$M_r = 855.21$
Orthorhombic, *Pbcn*
$a = 12.8038$ (8) Å
$b = 10.1729$ (4) Å
$c = 27.9377$ (14) Å
$V = 3638.9$ (3) Å^3
$Z = 4$
$F(000) = 1720$
$D_x = 1.561$ Mg m^{-3}
Mo $K\alpha$ radiation, $\lambda = 0.71073$ Å
Cell parameters from 1992 reflections
$\theta = 2.6$–$21.9°$
$\mu = 2.78$ mm^{-1}
$T = 200$ K
Plate, clear colourless
0.3 × 0.2 × 0.03 mm

Data collection

Xcalibur, Eos diffractometer
Radiation source: fine-focus sealed X-ray tube, Enhance (Mo) X-ray Source
Graphite monochromator
Detector resolution: 16.1593 pixels mm^{-1}
ω scans
Absorption correction: multi-scan (CrysAlisPro; Rigaku OD, 2024)
$T_{min} = 0.534$, $T_{max} = 1.000$
11620 measured reflections
3218 independent reflections
2074 reflections with $I > 2\sigma(I)$
$R_{int} = 0.064$
$\theta_{max} = 25.0°$, $\theta_{min} = 2.2°$
$h = -8\rightarrow15$
$k = -12\rightarrow12$
$l = -33\rightarrow23$

Refinement

Refinement on F^2
Least-squares matrix: full
$R[F^2 > 2\sigma(F^2)] = 0.061$
$wR(F^2) = 0.134$
$S = 1.03$
3218 reflections
236 parameters
0 restraints
Primary atom site location: dual
Hydrogen site location: mixed
H atoms treated by a mixture of independent and constrained refinement
$w = 1/[\sigma^2(F_o^2) + (0.042P)^2 + 6.2503P]$ where $P = (F_o^2 + 2F_c^2)/3$
$(\Delta/\sigma)_{max} < 0.001$
$\Delta\rho_{max} = 0.74$ e Å^{-3}
$\Delta\rho_{min} = -0.81$ e Å^{-3}

Special details

Geometry. All esds (except the esd in the dihedral angle between two l.s. planes) are estimated using the full covariance matrix. The cell esds are taken into account individually in the estimation of esds in distances, angles and torsion angles; correlations between esds in cell parameters are only used when they are defined by crystal symmetry. An approximate (isotropic) treatment of cell esds is used for estimating esds involving l.s. planes.

Fractional atomic coordinates and isotropic or equivalent isotropic displacement parameters (Å²)

	x	*y*	*z*	U_{iso}*/U_{eq}
Br1	0.66307 (8)	0.02071 (7)	0.48878 (3)	0.0797 (4)
Ni1	0.500000	0.70049 (8)	0.750000	0.0216 (2)
N1	0.5117 (3)	0.8456 (4)	0.80613 (15)	0.0256 (10)
N2	0.6139 (3)	0.8692 (4)	0.81923 (16)	0.0248 (10)
N3	0.6556 (3)	0.7082 (4)	0.76558 (14)	0.0219 (10)
N4	0.5627 (3)	0.5623 (4)	0.70264 (15)	0.0231 (10)
N5	0.5333 (3)	0.4789 (4)	0.66679 (15)	0.0251 (10)
N6	0.7063 (3)	0.4515 (4)	0.67934 (16)	0.0259 (10)
C1	0.4561 (4)	0.9206 (5)	0.83493 (19)	0.0301 (13)
H1	0.381986	0.925804	0.834432	0.036*
C2	0.5201 (5)	0.9917 (5)	0.8664 (2)	0.0390 (16)
H2	0.498267	1.051486	0.890526	0.047*
C3	0.6200 (5)	0.9572 (5)	0.8552 (2)	0.0335 (14)
H3	0.681998	0.988952	0.869887	0.040*
C4	0.6923 (4)	0.7938 (5)	0.79686 (18)	0.0241 (12)
C5	0.7978 (4)	0.8087 (5)	0.80651 (19)	0.0325 (14)
H5	0.822350	0.871958	0.828859	0.039*
C6	0.8649 (4)	0.7276 (5)	0.7822 (2)	0.0377 (15)
H6	0.938019	0.735362	0.787377	0.045*
C7	0.8278 (4)	0.6343 (5)	0.7501 (2)	0.0349 (14)
H7	0.874470	0.577053	0.733845	0.042*
C8	0.7215 (4)	0.6267 (5)	0.74235 (18)	0.0237 (12)
C9	0.6658 (4)	0.5433 (5)	0.70830 (18)	0.0237 (12)
C10	0.6212 (4)	0.4151 (5)	0.65395 (19)	0.0260 (13)
C11	0.6278 (4)	0.3207 (5)	0.61459 (19)	0.0275 (13)
C12	0.7116 (5)	0.2340 (5)	0.6123 (2)	0.0380 (15)
H12	0.762148	0.235364	0.637192	0.046*
C13	0.7239 (5)	0.1457 (6)	0.5749 (2)	0.0470 (17)
H13	0.782299	0.088134	0.573719	0.056*
C14	0.6488 (5)	0.1440 (5)	0.5396 (2)	0.0403 (16)
C15	0.5639 (5)	0.2259 (5)	0.5405 (2)	0.0414 (16)
H15	0.513185	0.222718	0.515651	0.050*
C16	0.5530 (5)	0.3147 (5)	0.57862 (19)	0.0345 (14)
H16	0.494019	0.371228	0.579850	0.041*
O1	0.3537 (4)	0.5660 (5)	0.61938 (19)	0.0542 (14)
H1A	0.397 (5)	0.548 (6)	0.635 (2)	0.05 (2)*
C17	0.3843 (6)	0.6447 (6)	0.5808 (3)	0.070 (2)
H17A	0.404825	0.588562	0.553908	0.105*
H17B	0.443564	0.699591	0.590398	0.105*

H17C	0.325855	0.700940	0.571141	0.105*

Atomic displacement parameters (Å²)

	U^{11}	U^{22}	U^{33}	U^{12}	U^{13}	U^{23}
Br1	0.1213 (9)	0.0692 (5)	0.0486 (5)	0.0147 (5)	−0.0015 (5)	−0.0307 (4)
Ni1	0.0135 (5)	0.0257 (5)	0.0254 (5)	0.000	−0.0008 (5)	0.000
N1	0.016 (3)	0.031 (2)	0.030 (2)	0.001 (2)	−0.006 (2)	0.0002 (19)
N2	0.014 (2)	0.028 (2)	0.032 (3)	0.0003 (19)	−0.002 (2)	−0.005 (2)
N3	0.016 (2)	0.022 (2)	0.028 (2)	−0.0013 (19)	−0.001 (2)	−0.0033 (18)
N4	0.018 (3)	0.026 (2)	0.025 (2)	−0.0010 (19)	−0.001 (2)	−0.0036 (18)
N5	0.019 (3)	0.030 (2)	0.026 (2)	−0.003 (2)	0.000 (2)	−0.0039 (19)
N6	0.017 (2)	0.028 (2)	0.033 (3)	−0.0011 (19)	0.003 (2)	−0.0058 (19)
C1	0.022 (3)	0.037 (3)	0.031 (3)	0.005 (3)	0.002 (3)	0.001 (2)
C2	0.037 (4)	0.045 (4)	0.035 (3)	0.010 (3)	0.006 (3)	−0.013 (3)
C3	0.027 (3)	0.037 (3)	0.036 (3)	0.000 (3)	−0.006 (3)	−0.015 (3)
C4	0.019 (3)	0.023 (3)	0.030 (3)	0.003 (2)	−0.004 (3)	−0.002 (2)
C5	0.024 (3)	0.041 (3)	0.032 (3)	−0.002 (3)	−0.006 (3)	−0.014 (3)
C6	0.016 (3)	0.050 (4)	0.047 (4)	0.001 (3)	−0.007 (3)	−0.010 (3)
C7	0.018 (3)	0.044 (3)	0.043 (4)	0.003 (3)	0.001 (3)	−0.015 (3)
C8	0.019 (3)	0.029 (3)	0.023 (3)	−0.001 (2)	0.000 (3)	0.000 (2)
C9	0.015 (3)	0.029 (3)	0.027 (3)	−0.002 (2)	−0.002 (3)	0.000 (2)
C10	0.025 (3)	0.025 (3)	0.028 (3)	−0.005 (2)	−0.001 (3)	0.001 (2)
C11	0.029 (3)	0.027 (3)	0.026 (3)	−0.003 (2)	0.004 (3)	0.001 (2)
C12	0.039 (4)	0.041 (3)	0.033 (3)	0.003 (3)	−0.007 (3)	−0.008 (3)
C13	0.050 (5)	0.046 (4)	0.045 (4)	0.014 (3)	0.006 (4)	−0.006 (3)
C14	0.062 (5)	0.028 (3)	0.031 (3)	0.002 (3)	0.006 (4)	−0.006 (2)
C15	0.053 (4)	0.042 (4)	0.028 (3)	−0.005 (3)	−0.004 (3)	−0.003 (3)
C16	0.037 (4)	0.029 (3)	0.038 (3)	−0.001 (3)	−0.003 (3)	0.002 (3)
O1	0.032 (3)	0.073 (3)	0.058 (3)	−0.004 (3)	−0.009 (3)	0.026 (3)
C17	0.094 (7)	0.054 (4)	0.063 (5)	−0.014 (4)	−0.021 (5)	0.015 (4)

Geometric parameters (Å, º)

Br1—C14	1.903 (5)	C5—H5	0.9500
Ni1—N1^{i}	2.159 (4)	C5—C6	1.372 (7)
Ni1—N1	2.159 (4)	C6—H6	0.9500
Ni1—N3	2.041 (4)	C6—C7	1.390 (7)
Ni1—N3^{i}	2.041 (4)	C7—H7	0.9500
Ni1—N4^{i}	2.091 (4)	C7—C8	1.380 (7)
Ni1—N4	2.091 (4)	C8—C9	1.461 (7)
N1—N2	1.380 (5)	C10—C11	1.462 (7)
N1—C1	1.318 (6)	C11—C12	1.390 (7)
N2—C3	1.347 (6)	C11—C16	1.389 (7)
N2—C4	1.409 (6)	C12—H12	0.9500
N3—C4	1.320 (6)	C12—C13	1.386 (8)
N3—C8	1.349 (6)	C13—H13	0.9500
N4—N5	1.366 (5)	C13—C14	1.378 (8)

N4—C9	1.344 (6)	C14—C15	1.370 (8)
N5—C10	1.348 (6)	C15—H15	0.9500
N6—C9	1.339 (6)	C15—C16	1.404 (7)
N6—C10	1.352 (6)	C16—H16	0.9500
C1—H1	0.9500	O1—H1A	0.73 (6)
C1—C2	1.403 (7)	O1—C17	1.398 (8)
C2—H2	0.9500	C17—H17A	0.9800
C2—C3	1.364 (7)	C17—H17B	0.9800
C3—H3	0.9500	C17—H17C	0.9800
C4—C5	1.386 (7)		

N1—Ni1—N1^{i}	93.7 (2)	C6—C5—C4	116.7 (5)
N3—Ni1—N1^{i}	101.33 (16)	C6—C5—H5	121.7
N3^{i}—Ni1—N1	101.33 (16)	C5—C6—H6	119.5
N3^{i}—Ni1—N1^{i}	75.58 (16)	C5—C6—C7	121.0 (5)
N3—Ni1—N1	75.58 (16)	C7—C6—H6	119.5
N3^{i}—Ni1—N3	175.6 (2)	C6—C7—H7	120.8
N3—Ni1—N4	77.64 (16)	C8—C7—C6	118.5 (5)
N3^{i}—Ni1—N4	105.42 (16)	C8—C7—H7	120.8
N3^{i}—Ni1—N4^{i}	77.64 (16)	N3—C8—C7	120.4 (5)
N3—Ni1—N4^{i}	105.42 (16)	N3—C8—C9	111.5 (5)
N4^{i}—Ni1—N1^{i}	153.21 (16)	C7—C8—C9	128.0 (5)
N4—Ni1—N1	153.21 (16)	N4—C9—C8	118.2 (4)
N4—Ni1—N1^{i}	91.54 (16)	N6—C9—N4	114.2 (4)
N4^{i}—Ni1—N1	91.54 (16)	N6—C9—C8	127.6 (5)
N4^{i}—Ni1—N4	95.5 (2)	N5—C10—N6	113.6 (4)
N2—N1—Ni1	112.2 (3)	N5—C10—C11	124.4 (5)
C1—N1—Ni1	143.3 (4)	N6—C10—C11	121.9 (5)
C1—N1—N2	104.5 (4)	C12—C11—C10	119.7 (5)
N1—N2—C4	117.6 (4)	C16—C11—C10	122.2 (5)
C3—N2—N1	111.6 (4)	C16—C11—C12	118.1 (5)
C3—N2—C4	130.6 (5)	C11—C12—H12	118.9
C4—N3—Ni1	120.9 (3)	C13—C12—C11	122.2 (6)
C4—N3—C8	120.2 (4)	C13—C12—H12	118.9
C8—N3—Ni1	118.9 (3)	C12—C13—H13	121.1
N5—N4—Ni1	140.9 (3)	C14—C13—C12	117.9 (6)
C9—N4—Ni1	113.6 (3)	C14—C13—H13	121.1
C9—N4—N5	105.5 (4)	C13—C14—Br1	118.4 (5)
C10—N5—N4	105.3 (4)	C15—C14—Br1	119.3 (5)
C9—N6—C10	101.3 (4)	C15—C14—C13	122.3 (5)
N1—C1—H1	124.3	C14—C15—H15	120.6
N1—C1—C2	111.4 (5)	C14—C15—C16	118.9 (6)
C2—C1—H1	124.3	C16—C15—H15	120.6
C1—C2—H2	127.1	C11—C16—C15	120.6 (5)
C3—C2—C1	105.8 (5)	C11—C16—H16	119.7
C3—C2—H2	127.1	C15—C16—H16	119.7
N2—C3—C2	106.7 (5)	C17—O1—H1A	112 (5)
N2—C3—H3	126.6	O1—C17—H17A	109.5

C2—C3—H3	126.6	O1—C17—H17B	109.5
N3—C4—N2	113.6 (4)	O1—C17—H17C	109.5
N3—C4—C5	123.2 (5)	H17A—C17—H17B	109.5
C5—C4—N2	123.2 (5)	H17A—C17—H17C	109.5
C4—C5—H5	121.7	H17B—C17—H17C	109.5

Br1—C14—C15—C16	178.8 (4)	C1—N1—N2—C4	175.0 (4)
Ni1—N1—N2—C3	−178.2 (3)	C1—C2—C3—N2	−0.6 (6)
Ni1—N1—N2—C4	−3.0 (5)	C3—N2—C4—N3	174.0 (5)
Ni1—N1—C1—C2	176.8 (4)	C3—N2—C4—C5	−6.4 (9)
Ni1—N3—C4—N2	3.7 (6)	C4—N2—C3—C2	−173.9 (5)
Ni1—N3—C4—C5	−175.9 (4)	C4—N3—C8—C7	−1.7 (7)
Ni1—N3—C8—C7	176.4 (4)	C4—N3—C8—C9	−178.1 (4)
Ni1—N3—C8—C9	0.1 (5)	C4—C5—C6—C7	−0.9 (9)
Ni1—N4—N5—C10	−177.8 (4)	C5—C6—C7—C8	1.4 (9)
Ni1—N4—C9—N6	177.7 (3)	C6—C7—C8—N3	−0.1 (8)
Ni1—N4—C9—C8	−5.4 (6)	C6—C7—C8—C9	175.6 (5)
N1—N2—C3—C2	0.5 (6)	C7—C8—C9—N4	−172.4 (5)
N1—N2—C4—N3	−0.2 (6)	C7—C8—C9—N6	4.0 (9)
N1—N2—C4—C5	179.4 (5)	C8—N3—C4—N2	−178.2 (4)
N1—C1—C2—C3	0.5 (7)	C8—N3—C4—C5	2.2 (8)
N2—N1—C1—C2	−0.2 (6)	C9—N4—N5—C10	0.6 (5)
N2—C4—C5—C6	179.5 (5)	C9—N6—C10—N5	−0.8 (6)
N3—C4—C5—C6	−0.9 (8)	C9—N6—C10—C11	175.8 (5)
N3—C8—C9—N4	3.6 (6)	C10—N6—C9—N4	1.2 (6)
N3—C8—C9—N6	180.0 (5)	C10—N6—C9—C8	−175.3 (5)
N4—N5—C10—N6	0.1 (6)	C10—C11—C12—C13	−177.6 (5)
N4—N5—C10—C11	−176.4 (4)	C10—C11—C16—C15	177.7 (5)
N5—N4—C9—N6	−1.2 (6)	C11—C12—C13—C14	−1.0 (9)
N5—N4—C9—C8	175.7 (4)	C12—C11—C16—C15	−1.7 (8)
N5—C10—C11—C12	−162.1 (5)	C12—C13—C14—Br1	−178.7 (4)
N5—C10—C11—C16	18.4 (8)	C12—C13—C14—C15	0.1 (9)
N6—C10—C11—C12	21.6 (8)	C13—C14—C15—C16	0.0 (9)
N6—C10—C11—C16	−157.8 (5)	C14—C15—C16—C11	0.9 (8)
C1—N1—N2—C3	−0.2 (6)	C16—C11—C12—C13	1.8 (9)

Symmetry code: (i) −*x*+1, *y*, −*z*+3/2.

Hydrogen-bond geometry (Å, º)

Cg is the centroid of the C11–C16 ring.

D—H···*A*	*D*—H	H···*A*	*D*···*A*	*D*—H···*A*
C3—H3···O1^{ii}	0.95	2.35	3.269 (8)	162
C5—H5···O1^{ii}	0.95	2.48	3.413 (7)	167
C1—H1···N6^{iii}	0.95	2.30	3.238 (6)	171
C7—H7···C1^{iv}	0.95	2.71	3.615 (7)	161

O1—H1*A*···N5	0.73 (6)	2.08 (6)	2.798 (6)	168 (6)
C2—H2···*Cg*^{v}	0.95	2.69	3.542 (6)	140

Symmetry codes: (ii) *x*+1/2, *y*+1/2, −*z*+3/2; (iii) *x*−1/2, *y*+1/2, −*z*+3/2; (iv) *x*+1/2, *y*−1/2, −*z*+3/2; (v) −*x*+1, *y*+1, −*z*+3/2.

Hydrogen-bond geometry (Å, °)

D*–*H*···*A	***D*–*H***	***H*···*A***	***D*···*A***	***D*–*H*···*A***
C3–H3···O1^{i}	0.95	2.35	3.268 (7)	162
C5–H5···O1^{i}	0.95	2.48	3.410 (7)	167
C1–H1···N6^{ii}	0.95	2.30	3.238 (6)	171
C7–H7···C1^{ii}	0.95	2.71	3.615 (7)	161
O1–H1A···N5	0.73 (6)	2.08 (6)	2.798 (6)	168 (6)

Symmetry codes: (i) 1/2 + x, 1/2 + y, 1.5 - z; (ii) 1/2 + x, -1/2 + y, 1.5 - z